Environmental Science & Technology

Article

pubs.acs.org/est

Airborne Ethane Observations in the Barnett Shale: Quantification of Ethane Flux and Attribution of Methane Emissions

Mackenzie L. Smith,[†] Eric A. Kort,*[,†] Anna Karion,[‡,§] Colm Sweeney,[‡,§] Scott C. Herndon,[∥] and Tara I. Yacovitch[∥]

[†]Atmospheric, Oceanic, and Space Sciences, University of Michigan, Ann Arbor, Michigan 48109, United States

[‡]CIRES, University of Colorado, Boulder, Colorado 80309, United States

[§]NOAA Earth System Research Laboratory, Boulder, Colorado 80305, United States

[∥]Aerodyne Research, Inc., Billerica, Massachusetts 01821, United States

Supporting Information

ABSTRACT: We present high time resolution airborne ethane (C_2H_6) and methane (CH_4) measurements made in March and October 2013 as part of the Barnett Coordinated Campaign over the Barnett Shale formation in Texas. Ethane fluxes are quantified using a downwind flight strategy, a first demonstration of this approach for C_2H_6. Additionally, ethane-to-methane emissions ratios (C_2H_6:CH_4) of point sources were observationally determined from simultaneous airborne C_2H_6 and CH_4 measurements during a survey flight over the source region. Distinct C_2H_6:CH_4 × 100% molar ratios of 0.0%, 1.8%, and 9.6%, indicative of microbial, low-C_2H_6 fossil, and high-C_2H_6 fossil sources, respectively, emerged in observations over the emissions source region of the Barnett Shale. Ethane-to-methane correlations were used in conjunction with C_2H_6 and CH_4 fluxes to quantify the fraction of CH_4 emissions derived from fossil and microbial sources. On the basis of two analyses, we find 71−85% of the observed methane emissions quantified in the Barnett Shale are derived from fossil sources. The average ethane flux observed from the studied region of the Barnett Shale was 6.6 ± 0.2 × 10^3 kg hr^{-1} and consistent across six days in spring and fall of 2013.

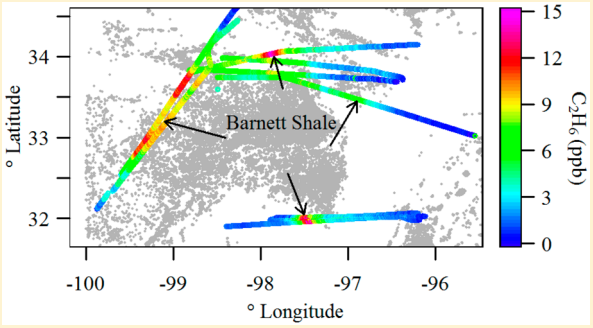

INTRODUCTION

Methane (CH_4) is an important greenhouse gas (GHG) that influences climate and affects atmospheric chemistry as a precursor for tropospheric ozone production.[1] Inventory-based estimates suggest that fossil fuel extraction, distribution, and processing are the most significant sources of anthropogenic methane emissions in the United States.[2] However, quantification and partitioning of CH_4 enhancements between fossil fuel-related activities and methane's other major sources, predominantly microbial, which include agriculture, landfills, and wetlands, have proven difficult for past and present emissions estimates and on regional, national, and global scales.[3−7] This difficulty is reflected in the persistent disagreement between bottom-up (ground-based inventory) and top-down (airborne-based) estimates of CH_4 emissions

Previous efforts to quantify and apportion CH_4 emissions between fossil fuel and microbial sources have utilized carbon-13 isotopes (^{13}C:^{12}C is enriched in fossil fuel-derived carbon compared to carbon produced by microbial activity) and nonmethane hydrocarbons (NMHCs) such as ethane (C_2H_6) and propane (C_3H_8), which are primarily emitted from fossil fuel sources as tracer species.[8−13] Ethane is a useful tracer for fossil fuel-derived CH_4 because it is not emitted by methane's microbial sources. Major global sources of C_2H_6 are the oil and gas sector (8−9.2 Tg yr^{-1}), biofuel production and use (2.6 Tg yr^{-1}), and biomass burning (2.4−2.8 Tg yr^{-1}).[3,13−15] Ethane is also an important trace gas from a regional atmospheric chemistry perspective because of the role it can play in days subsequent to its release in enhancing regional tropospheric ozone concentrations and peroxyactyl nitrate production by way of its reaction with the hydroxyl radical (OH).[1,16,17]

To date, most measurements of atmospheric C_2H_6 have utilized offline analyses from whole-air or flask samples. Global concentrations and emissions rates of NMHCs including C_2H_6 have been determined from worldwide networks of whole-air samples[11−13] and on smaller scales using whole-air samples from both ground-based and airborne platforms,[10,18−20] often with the goal of attributing CH_4 emissions to different source sectors. When used for attribution, whole-air samples may be well suited for characterization of static or regional sources, but limitations in the frequency and speed with which samples can be collected and analyzed means that they are not ideal for observations of narrow plumes or quickly changing emissions

Received: December 9, 2014
Revised: April 15, 2015
Accepted: May 27, 2015
Published: July 7, 2015

DOI: 10.1021/acs.est.5b00219
Environ. Sci. Technol. 2015, 49, 8158−8166

Table 1. C_2H_6 Fluxes, CH_4 Fluxes, and C_2H_6:CH_4 for All Downwind Mass Balance Flights[a]

date	$flux_{CH4}$ ($\times 10^3$ kg hr^{-1}; Karion et al.[24])	$flux_{CH4}$ ($\times 10^3$ kg hr^{-1})	$flux_{C2H6}$ ($\times 10^3$ kg hr^{-1})	$flux_{C2H6}$: $flux_{CH4}$ (mol:mol × 100)	no. of transects	V (m s^{-1})	Θ (deg)	PBL (magl)
27-03-13	87	93 ± 48	6.3 ± 3.5	3.6 ± 0.8	1	11.6	180	1500
30-03-13	78	59 ± 30	6.5 ± 3.8	5.9 ± 0.8	1	6.0	225	1260
16-10-13	41	55 ± 15	6.4 ± 2.0	6.2 ± 0.4	2	7.6	8	670
19-10-13	61	60 ± 19	6.8 ± 2.4	6.0 ± 0.5	5	5.6	344	1011
20-10-13	88	92 ± 55	6.7 ± 4.0	3.9 ± 0.9	2	6.6	171	933
25-10-13	109	113 ± 49	16.4 ± 7.0	7.4 ± 0.6	2	6.0	150	705
28-10-13	64	80 ± 41	6.6 ± 3.6	4.4 ± 0.7	2	5.2	156	660
mean:[b]	76 ± 13	74 ± 18	6.6 ± 0.2	5.0 ± 1.2				

[a]Data shown are averages for all transects flown on a given day. [b]Means for columns exclude data from 25-Oct. (data from 25-Oct. is included in the mean of Karion et al.,[24] column 2). Uncertainties on daily average values are determined as described in the Methods section. The standard deviation of the means is taken as the uncertainty on the mean values for the region.

encountered from an airborne platform. In a field where variable amounts of tracer species (such as C_2H_6) relative to CH_4 are emitted from different sources, correlations or emissions ratios based on flask samples can be misleading. We illustrate this in Figure S1 of the Supporting Information for the Barnett Shale, demonstrating that subsampling the C_2H_6:CH_4 ratio on the airborne data set results in a calculated C_2H_6:CH_4 ratio not representative of any emission ratio seen. We therefore advise caution in interpreting limited air samples.

In contrast, the recently developed C_2H_6 laser absorption spectrometer measures C_2H_6 mole fractions with a 1 Hz frequency and subppb precision,[21] making possible characterization from rapidly changing sources and tightly constrained emissions estimates of C_2H_6 regional fluxes. When paired with simultaneous CH_4 measurements, the continuous in situ airborne observations of C_2H_6 provide a new and useful method for attribution of CH_4 emissions to specific source sectors.

Herein, we present the first C_2H_6 emissions estimates from a region of high gas and oil production over the Barnett Shale formation in Texas, using high resolution airborne C_2H_6 measurements and a mass balance flight strategy. Measurements were collected as part of the larger Barnett Coordinated Campaign designed to investigate methane emissions from the Barnett shale formation. The studied emissions source region was defined as the eight counties (Dallas, Johnson, Tarrant, Wise, Denton, Parker, Hood, and Montague) within which about 92% of gas production in the region occurs.[22,23] These counties, bounded by about −98° to −96.5° longitude and 32° to 34° latitude, were covered during all downwind mass balance flights. Using concurrent airborne measurements of CH_4, ratios of ethane-to-methane emissions (C_2H_6:CH_4) of specific CH_4 emissions sources were also studied on a survey flight over the source region. In combination with CH_4 fluxes,[24] the measured C_2H_6 fluxes and the distribution of C_2H_6:CH_4 over the source region enable partitioning of CH_4 emitted between biogenic and fossil fuel sources.

METHODS

Instrumentation. An airborne measurement campaign was conducted onboard a Mooney aircraft (Scientific Aviation, Inc.) over the Barnett Shale region in Texas in March and October 2013. An Aerodyne ethane laser absorption spectrometer was deployed on the aircraft and quantified C_2H_6 mixing ratios with a 1 Hz data acquisition frequency. The major components of the C_2H_6 spectrometer are a tunable mid-infrared (3.3 μm) diode laser, a multipass absorption sample cell, and an infrared detector. Details regarding the theory and operation of the C_2H_6 spectrometer are described by Yacovitch et al.[21] Additional instrumentation and airborne measurements, including CH_4 and H_2O mole fractions (Picarro, G2401-m, cavity ring-down spectroscopy; ∼0.5 Hz data acquisition frequency), wind speed and direction, GPS location, and ambient temperature and pressure, are described by Karion et al.[24]

Under the operational conditions of the field deployment, the C_2H_6 instrument time response was about 600 ms, and the in-flight 1 s precision was about 0.08 ppb. Spectral background scans were done every 15 min using ultra-zero air to minimize spectral drift. The instrument records wet C_2H_6 mole fraction, which is corrected to dry-air mole fraction utilizing H_2O vapor measured by the Picarro. The stability of the instrument during flight was tested by comparing C_2H_6 mole fractions measured in the free troposphere at the beginning and end of a flight. Free troposphere measurements of the C_2H_6 mole fraction were taken at altitudes above the mixed layer during vertical profiles conducted to determine boundary layer height. In this analysis, we assume the concentration of C_2H_6 in the free troposphere remained stable for the almost 4 h duration of a flight. The C_2H_6 values measured about 4 h apart on 19-Oct. were 1.10 ± 0.06 and 1.11 ± 0.07 ppb. This is supportive evidence that in-flight drift varied within the instrument precision during a typical research flight.

The accuracy of the C_2H_6 instrument relative to known standard scales was investigated by comparing the measured C_2H_6 in a tank of compressed air with that quantified by gas chromatography with flame ionization detection (GC-FID).[25] The absolute spectroscopy-determined value measured by this instrument underestimated the mole fraction measured by GC-FID (17.57 ppb) by 3%. Herein, we report the spectroscopic C_2H_6 values; however, if combining these C_2H_6 observations with other C_2H_6 data sets, this calibration offset must be accounted for.

Flux Calculations. Measurements of C_2H_6 mole fraction enhancements downwind of the source region were obtained on seven flights conducted on days when the wind speeds and directions were stable for about 18 h prior to flight. Winds were considered stable if back trajectories, constructed using Weather Research and Forecasting (WRF) winds, indicated that the air intercepted by a downwind flight transect originated upwind and outside of the source region and if the wind direction varied by less than 45° as the air mass transited across the source region. Fluxes are calculated from the downwind

DOI: 10.1021/acs.est.5b00219
Environ. Sci. Technol. 2015, 49, 8158−8166

enhancements in C_2H_6 mole fraction using the mass balance method, according to eq 1:

$$\text{flux}_{C2H6} = V \int_{-b}^{b} \Delta X_{C2H6} \left(\int_{z_{ground}}^{z_{PBL}} n_{air} dz \right) \cos\theta \, dx \quad (1)$$

where ΔX_{C2H6} is the molar enhancement of C_2H_6 above background concentrations, $-b$ to b is the width of the enhancement plume, z_{ground} to z_{PBL} is the height of the planetary boundary layer (PBL), and $V \cos\theta$ is the component of uniform horizontal wind speed perpendicular to the flight path. This mass balance method has been used to quantify emissions from point and regional sources,[19,26] although this is the first application to C_2H_6 fluxes. The CH_4 fluxes for each flight are also calculated here for comparison with those of Karion et al.,[24] and they agree within the uncertainty bounds for each individual transect and the average total CH_4 emissions from the Barnett region (Table 1). Differences between the fluxes of Karion et al. and this study are caused by using independently determined CH_4 backgrounds and PBL heights in eq 1 (wind speed and directions are taken from Karion et al.[24]). We use the CH_4 fluxes calculated herein in our analysis of CH_4 apportionment.

PBL heights are estimated from vertical profiles of H_2O and CH_4 mole fractions. Horizontal wind speeds and directions are obtained from modeled WRF winds averaged within the PBL and over the transit time of the air mass across the source region to the location of the downwind flight path (Supporting Information and Karion et al.[24]). Background concentrations of C_2H_6 and CH_4 are determined using a linear fit to the mean values observed at the plume edges (Figure 1).

Uncertainty in PBL height is assigned as the maximum difference between heights of different PBL estimates during a flight. The 1 s precision of 0.08 ppb is taken as the error on the C_2H_6 mole fraction measurement. Uncertainty in C_2H_6 background mole fraction is derived from the variability of the mole fraction at the plume edges. Errors in wind direction and speed, and CH_4 mole fractions and background values are given by Karion et al.[24] Uncertainties for each of the individual quantities included in eq 1 are summed in quadrature to obtain the error estimates on the C_2H_6 and CH_4 fluxes calculated for each downwind transect.

Use of eq 1 assumes that measurements at the altitude of the downwind transects are representative of the entire boundary layer. Downwind mass balance flights conducted at multiple altitudes support the validity of this assumption for C_2H_6 mole fractions (Figure S2, Supporting Information) and CH_4 mole fractions,[24] although a lack of complete vertical mixing and horizontal variability likely contribute to the variability among flux estimates determined from different transects.

C_2H_6:CH_4 of Emissions Sources. One flight on 17-Oct. directly over the emissions source region was conducted under conditions of low wind speed (< about 2 m s^{-1}) and variable wind direction (south or east) to characterize the C_2H_6:CH_4 of emissions from individual sources.[21] The C_2H_6:CH_4 values that characterize CH_4 emissions, and their spatial distribution over the source region, are determined by calculating the slopes (using orthogonal distance regression) of the C_2H_6-to-CH_4 relationships in two ways: Window Method and Plume Method. In order to compare C_2H_6 and CH_4 data, the 1 Hz C_2H_6 mole fraction time series was interpolated and mapped onto the time-stamp of the CH_4 data set because CH_4 mole fractions were reported at a lower frequency (about 0.5 Hz).

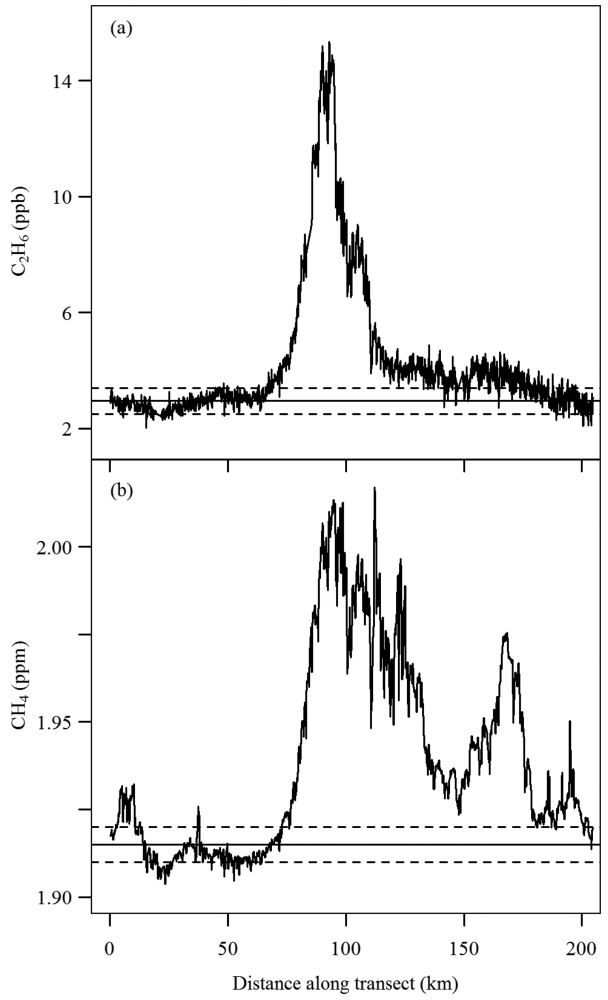

Figure 1. C_2H_6 (a) and CH_4 (b) observations in a downwind transect on 19-Oct. The background concentrations used in the flux calculations (solid lines) and the upper and lower uncertainty bounds on the background estimate (dotted lines) are also shown.

Window Method. The C_2H_6 and CH_4 observed over the source region include contributions from fresh emission plumes and broader background enhancements arising from mixing of older emissions. In our analysis, fresh emissions are isolated from mixed background enhancements by restricting analysis of C_2H_6:CH_4 slopes to changes in C_2H_6 and CH_4 over distances of less than or equal to 3 km (which corresponds to a 45 s window of data). To minimize the likelihood of including signals linked to small-scale atmospheric variability and nonlocal emissions, only data increments for which CH_4 mole fraction enhancements are greater than 10 ppb are included in the analysis.

The length scale of 3 km is chosen to avoid double-counting emissions plumes on multiple flight transects over the source region (which were spaced about 10−20 km apart); 3 km is the estimate for the horizontal diffusion of an air mass that has traveled about 10 km under the meteorological conditions of 17-Oct. (winds less than 2 ms^{-1} at the surface and high solar insolation).[27] The 45 s increments of data are sampled in 5 s intervals along the time series of C_2H_6 and CH_4. As an additional step to restrict analysis of C_2H_6:CH_4 to fresh CH_4 emissions, linear trends over the 45 s C_2H_6 and CH_4 time series increments are removed prior to the slope calculation to eliminate C_2H_6-to-CH_4 correlations over length scales greater

DOI: 10.1021/acs.est.5b00219
Environ. Sci. Technol. 2015, 49, 8158−8166

than or equal to 3 km. Examples of linearly detrended C_2H_6 and CH_4 time series increments, and the associated C_2H_6 vs CH_4 data and linear regression lines, are shown in Figure S3 of the Supporting Information.

To characterize total observed CH_4 emissions in the Barnett Shale region by a distribution of C_2H_6:CH_4 ratios, the frequency of each slope in the calculated data set is weighted by the integrated magnitude of the CH_4 enhancement over each increment to account for differences in emission sources. If the flight pattern over the field produced a representative random sampling of CH_4 emissions, potential positive or negative biases introduced by weighting the slope frequencies by the CH_4 enhancements (e.g., biases caused by sampling near or far from point sources) will cancel. The sampling representativeness is tested in the analysis presented in the section on Representativity of Source Field for Downwind Observations.

Plume Method. A second analysis of this same flight consists of selecting individual CH_4 plumes of width less than or equal to 3 km and a CH_4 enhancement greater than 10 ppb from the time series (this filter is chosen to ensure we are not fitting atmospheric variability but only plumes due to localized sources); a total of 108 plumes fit these criteria. For each plume, the slope is calculated (Figure S4, Supporting Information). The C_2H_6 and CH_4 time series are not detrended prior to the slope calculation. The integral of CH_4 is also calculated for each CH_4 plume and used to weight the frequency of each slope in the constructed histogram (Figure S5, Supporting Information).

For both methods, the *p*-value of the C_2H_6-to-CH_4 correlation is also calculated for each increment of data. The *p*-values describing the statistical significance of the C_2H_6-to-CH_4 correlations are used to filter the results of the slope analyses to obtain the amount of CH_4 enhancement observed over the source region that is significantly correlated with C_2H_6 (see the section on Attribution of CH_4 Emissions).

RESULTS AND DISCUSSION

C_2H_6 and CH_4 Fluxes. The emissions of C_2H_6 and CH_4 from the Barnett Shale source region are determined from the downwind measurements using the mass balance method (eq 1). Examples of C_2H_6 and CH_4 enhancement plumes observed on 19-Oct. are shown in Figure 1. One to five transects were flown on each of 7 days; the C_2H_6 and CH_4 fluxes calculated from each transect (Table S1, Supporting Information) are averaged to obtain daily estimates of emissions (Table 1).

Flight tracks showing the observed downwind C_2H_6 mole fractions for different wind directions are plotted in Figure 2. Downwind emissions were sampled from multiple directions surrounding the source region to test for biases from upwind sources. Additionally, to confirm similar CH_4 production, regions were sampled on each flight, and back trajectories from the downwind flight transects were modeled using WRF wind fields. Karion et al.[24] concluded that all seven flights sampled at least the eight counties of Dallas, Johnson, Tarrant, Wise, Denton, Parker, Hood, and Montague, covering 92% of gas production in the Barnett Shale region.

The daily average fluxes show a consistent day-to-day picture of C_2H_6 emissions, with the exception of 1 day: The $flux_{C2H6}$ of 16.4×10^3 kg hr^{-1} observed on 25-Oct. is over two times higher than any of the other daily averages. The larger C_2H_6 emissions observed on this flight are explained by the flight sampling emissions from a region further north and west than

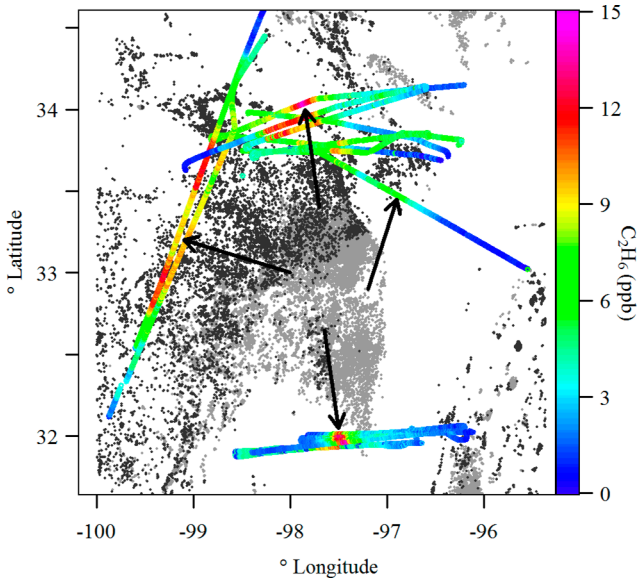

Figure 2. Downwind flight paths colored by observed C_2H_6 mole fraction on 27- and 30-March and 16-, 19-, 20-, 25-, and 28-Oct. Arrows indicate approximate wind directions for each flight (N for 16- and 19-Oct., SE for 25-Oct., S for 20- and 28-Oct. and 27-March, and SW for 30-March). The locations of gas-producing well pads (light gray) and liquid-producing well pads (black) are also shown. Wells are defined by the Texas Railroad Commission (Texas RRC) as primarily gas-producing if they produce greater than 100 thousand cubic feet (MCF) per day per barrel of hydrocarbon liquids per day.

was covered on other days (i.e., outside of the eight county source region), which resulted in higher liquids production coverage.[24] Data of 25-Oct. are therefore excluded from the averages for the eight-county source region (Table 1). On the basis of the remaining six days spanning two seasons (March and October 2013), the average C_2H_6 emissions from the Barnett region are 6.6 ± 0.2 ($\times 10^3$) kg hr^{-1}.The average CH_4 emissions calculated using data from the same six days are $74 \pm 18 \times 10^3$ kg hr^{-1}. This estimate agrees within error with the estimate of Karion et al.[24] of $76 \pm 13 \times 10^3$ kg hr^{-1}.We note that that the $flux_{CH4}$ value of Karion et al. is calculated using data from eight flights, including the flight of 25-Oct., and a flight on 25-March during which C_2H_6 was not measured. The standard deviation of the means is used as the uncertainty on the average flux estimates.

Across the six days used to determine fluxes from the region, no statistically significant variability in C_2H_6 emissions is observed. This finding strengthens the average flux results, as biases due to different upwind sources or transport conditions would not present in the same direction on different days with different wind directions. Furthermore, this indicates that although the Barnett Shale source region is complex and a range of activities varying from day-to-day contribute to CH_4 emissions over the entire field this variability appears to cancel and ethane emissions persist at a constant level.

Characterization of Methane Emissions by C_2H_6:CH_4. The spatial distributions of measured C_2H_6 concentrations and calculated C_2H_6:CH_4 values (as determined using the Window Method) over the source region are plotted in Figure 3 (see Figure S5, Supporting Information, for C_2H_6:CH_4 results of the Plume Method). Shown for comparison are liquid-producing well pad locations (where liquids = oil + condensate) and well pads producing primarily gas (defined as wells producing

DOI: 10.1021/acs.est.5b00219
Environ. Sci. Technol. 2015, 49, 8158−8166

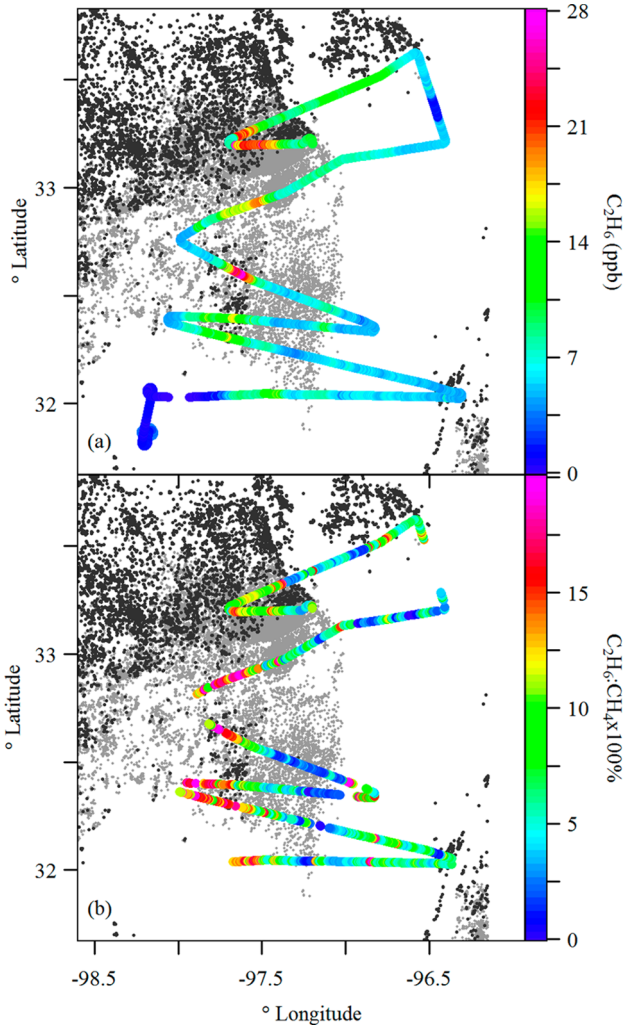

Figure 3. Flight path over emissions source region of the Barnett Shale on 17-Oct. Coloring along the flight path shows (a) C_2H_6 mole fraction or (b) C_2H_6:CH_4 determined using the Window Method. Wind direction is not indicated because wind speed was low (less than 2 ms^{-1}) and direction was variable. The locations of primarily gas-producing well pads (light gray) and liquid-producing well pads (black) are also shown.

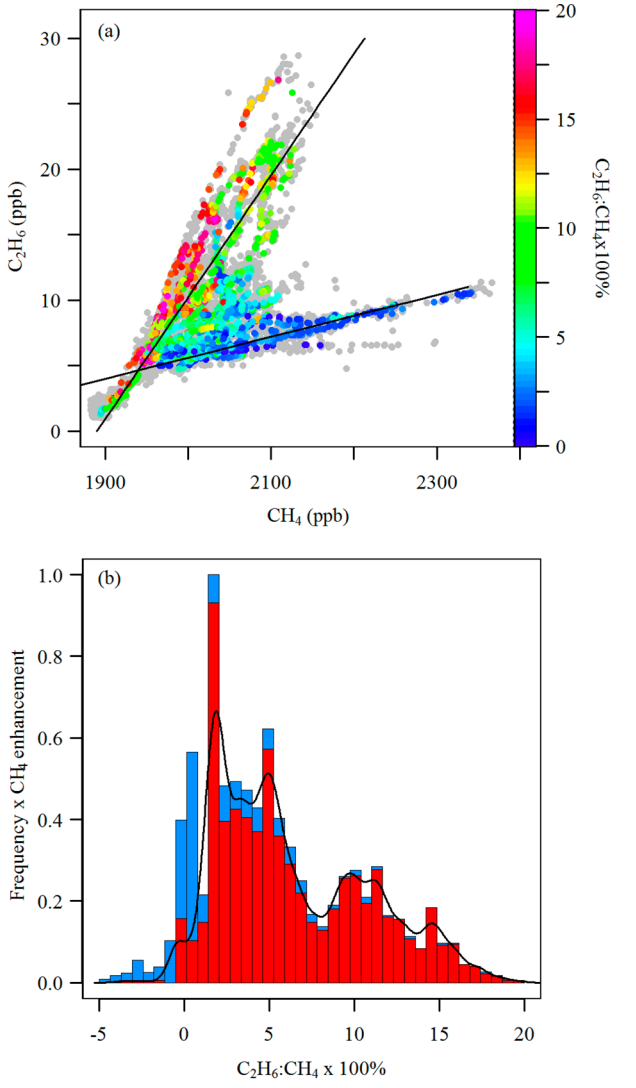

Figure 4. (a) C_2H_6 observations plotted against CH_4 observations of 17-Oct. The entire data set (gray points) and points colored by the slope calculated using the Window Method for each 45 s data increment are shown. Individual colored points are plotted as the median of C_2H_6 and CH_4 within each 45 s window analyzed. (b) Histogram of C_2H_6:CH_4 calculated using the Window Method. For each bin, the fraction of calculated slopes having a p-value ≤ 0.05 is shown in red, while the fraction associated with p-value > 0.05 is blue. The black line shows the PDF of the red data; the two local maxima of the PDF at 1.8 and 9.6 are used as the slopes of the lines shown in panel a. See the Methods section for further details on the analysis.

greater than 100 thousand cubic feet (MCF) per day per barrel of hydrocarbon liquids per day). The C_2H_6 and CH_4 concentrations are highest over regions with highest well density (see Figure 3 for C_2H_6 and Karion et al.[24] for CH_4). Both C_2H_6 and C_2H_6:CH_4 show peaks over areas of high liquid production, indicative that a high-C_2H_6 source of CH_4 emissions is associated with the wells producing large amounts of condensate or oil (i.e., "wet gas" wells). The lower values of C_2H_6:CH_4 (clustered around about 1−3%) are broadly distributed over the region and likely characterize emissions from fossil sources not associated with liquid production (i.e., "dry gas"). In addition to wells, the Barnett Shale contains a range of potential methane sources linked to natural gas activities, including gathering facilities and local distribution; all of these sources may be contributing to the "dry gas" signature. Processing plants may contribute to either the "dry" or "wet" signature. Nonfossil sources of methane present in the region (which do not produce ethane) include landfills and ruminants.

A plot of C_2H_6 against CH_4 observations from this flight (Figure 4a) reveals that there are two distinct predominant C_2H_6:CH_4 correlations over the source region. The 1 Hz C_2H_6 measurement, compared to low-temporal resolution measurements such as whole-air samples, is critical for resolving these multiple separate C_2H_6:CH_4 correlations. The histogram of slopes calculated for the fresh emissions using the Window Method (Figure 4b) shows approximately three distributions of CH_4 sources, consisting of a microbial source (C_2H_6:CH_4 × 100% = 0%) and two fossil fuel sources having maxima in C_2H_6:CH_4 × 100% at 1.8% and 9.6%. Repetition of the slope analysis using 90 and 180 s increments of data, rather than 45 s, reveals no significant differences in the shape of the slope histogram or the C_2H_6:CH_4 of the peaks (Figure S6, Supporting Information).

DOI: 10.1021/acs.est.5b00219
Environ. Sci. Technol. 2015, 49, 8158−8166

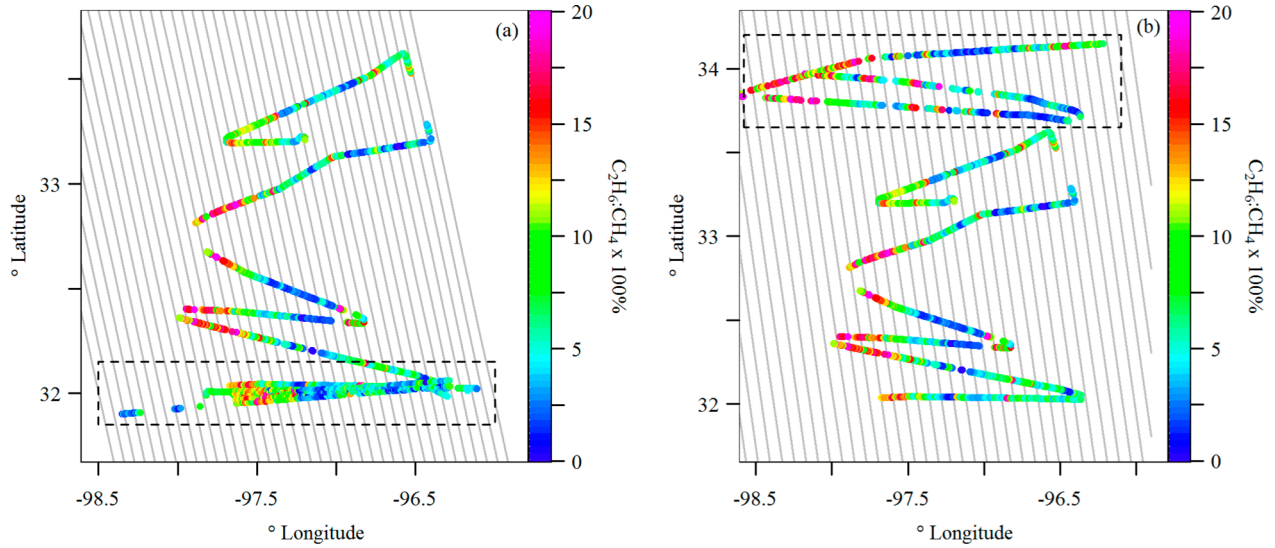

Figure 5. Flight paths colored by C_2H_6:CH_4 × 100% for the data of 17-Oct. (both panels) and either 19-Oct. (a) or 20-Oct. (b). Downwind transects of 19- or 20-Oct. are enclosed by the dashed line boxes. The 17-Oct. observations are averaged in sections defined by the gray lines, which are parallel to the wind direction on the 19 and 20-Oct., respectively.

The data of Figure 4a show features of the fresh enhancement plumes (points colored by slopes calculated over 45 s increments) and the older, mixed background enhancements (trends in C_2H_6:CH_4 correlations shown by the overall slopes of the gray points). The C_2H_6:CH_4 slopes calculated for the small-scale fresh emissions are similar to the larger overall trends in background enhancements (i.e., green points fall along the line of 9.6% slope, whereas blue points fall along the line of 1.8% slope).

Attribution of CH_4 Emissions. *Estimate of CH_4 Emissions from Fossil Fuel Sources.* Observations from the 17-Oct. flight are used to estimate the most likely attribution of CH_4 emissions to fossil fuel sources. The histograms of slopes that characterize CH_4 emissions sources (Figure 4 and Figure S5, Supporting Information) reveal information on the relative partitioning of CH_4 between fossil and nonfossil sources. We observe that there must be nonzero contributions to total CH_4 emissions from fossil fuel sources because a range of C_2H_6:CH_4 × 100% values greater than 0% prominently feature in the histograms (including dominant peaks at 9.6% and 1.8%) and nonthermogenic sources because CH_4 emissions not significantly correlated with C_2H_6 are observed (peak at 0%). We leverage this distinction in two approaches to partition source contributions between fossil and nonfossil emissions. We focus on the flight on 17-Oct. and consider the cumulative distribution function (CDF) of C_2H_6:CH_4 as one method (CDF-partitioning) and as a second method consider the significance of the correlations between C_2H_6 and CH_4 (p-value partitioning).

In the CDF-partitioning, the minimum between the peaks at 0% and 1.8% in the histogram is used to divide the CDF of C_2H_6:CH_4 × 100% (Window Method; Figure S7, Supporting Information) into two sources: microbial source (C_2H_6:CH_4 < 0.8%) and sum of fossil sources (C_2H_6:CH_4 ≥ 0.8%). For the Window Method, this partitions 15% to a microbial source and 85% to fossil sources. For the Plume Method C_2H_6:CH_4 × 100% histogram, this approach attributes 19% of the CH_4 enhancement to microbial sources and 81% to fossil sources.

In the p-value approach, the data of the histograms are filtered based on the p-value of the C_2H_6-to-CH_4 correlation to characterize plumes as either thermogenic or nonthermogenic (e.g., CH_4 plumes with and without associated C_2H_6). Methane enhancements within data increments associated with p-values > 0.05 (i.e., no C_2H_6-to-CH_4 correlation) are attributed to nonfossil sources, whereas enhancements associated with p-values ≤ 0.05 are attributed to fossil sources. Using the Window or Plume Methods, this approach attributes 19% or 29% of CH_4 emissions to microbial sources, respectively. Thus, the results of applying these two approaches to each of the slope histograms produce four estimates that attribute from 71% to 85% of the total CH_4 emissions from the Barnett Shale to fossil fuel sources.

Refined Methane Partitioning. Although it is clear that the CH_4 emissions are characterized by a range of C_2H_6:CH_4 × 100% between 0% and 20%, distinct values of 1.8% and 9.6% are observed in the plot of C_2H_6 vs CH_4 (Figure 4a). We thus consider a simple model where three source relations represent the Barnett emissions and quantitatively partition CH_4 between these three contributing sources (microbial source of 0%, low-C_2H_6 fossil fuel source of 1.8%, and high-C_2H_6 fossil source of 9.6%). Examples of possible low-C_2H_6 sources would be leaks of pipeline-grade natural gas or fugitive emissions of very clean unprocessed gas during drilling/production, whereas a high-C_2H_6 source could be fugitive emissions of unprocessed gas with higher ethane content or methane co-emitted along with higher alkanes from other sources such as condensate tanks. These are simply a few possibilities

Assuming the average downwind molar flux ratio $flux_{C2H6}$:$flux_{CH4}$ of 5.0% (Table 1) observed for the Barnett region is the result of a linear combination of the three assumed sources, we formulate (eq 2),

$$0\%f_M + 1.8\%f_{LE} + 9.6\%f_{HE} = 5.0\% \quad (2)$$

where f_M, f_{LE}, and f_{HE} are the fractions of microbial, low-C_2H_6 fossil fuel, and high-C_2H_6 fossil fuel, respectively, that contribute to the total CH_4 emissions. With three unknowns, eq 2 is under-constrained. However, upper/lower bounds on the relative contribution of each source can be found by using eq 2 and the constraints that $f_M + f_{LE} + f_{HE} = 1$ and all f are between zero and one (i.e., the fractions of CH_4 attributable to

DOI: 10.1021/acs.est.5b00219
Environ. Sci. Technol. 2015, 49, 8158−8166

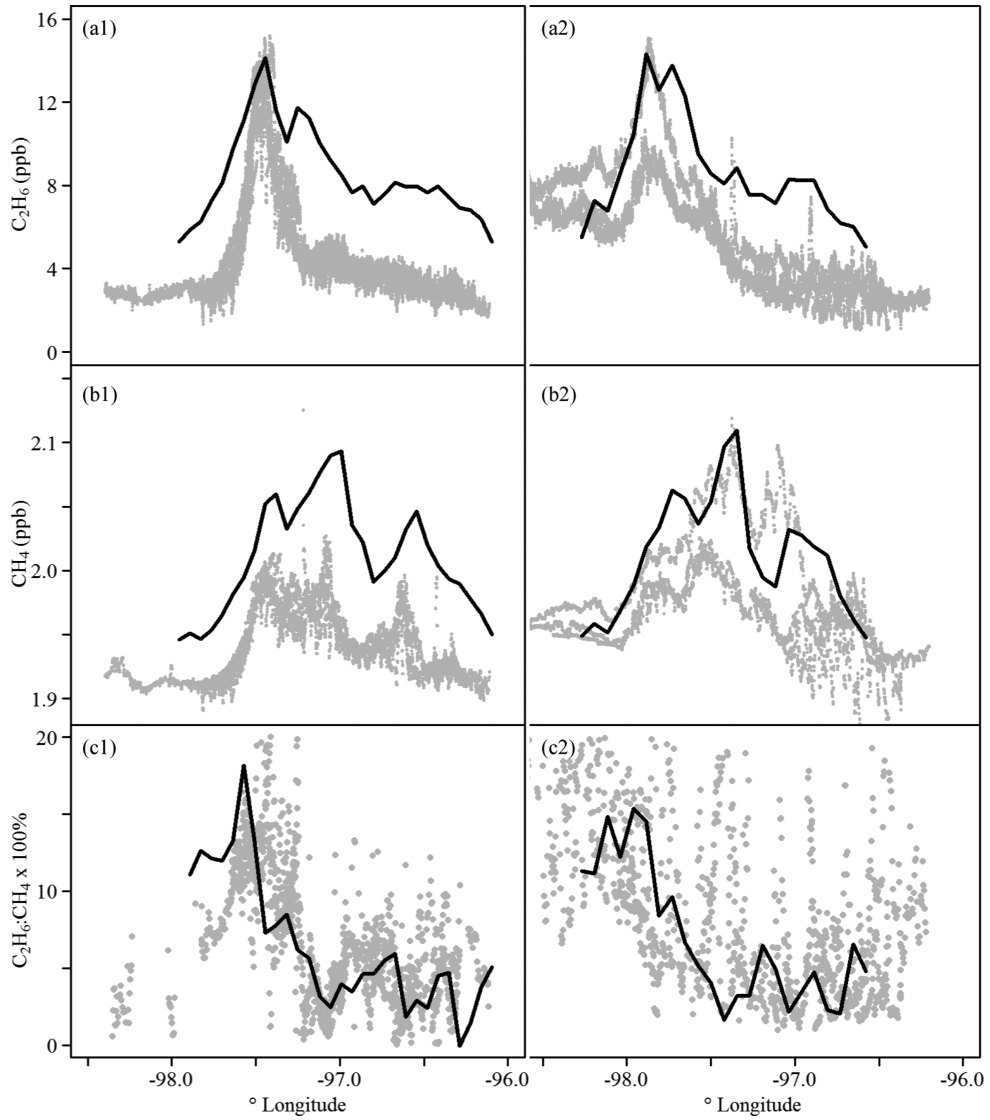

Figure 6. Simulated C_2H_6 (row a), CH_4 (row b), and C_2H_6:CH_4 × 100% (row c) in the downwind flight transects of 19-Oct. (column 1) and 20-Oct. (column 2). C_2H_6, CH_4, and C_2H_6:CH_4 × 100% observed in the downwind transects (gray points) are compared to the values simulated using data of 17-Oct.(lines).

each of the three sources are the ranges of f_M, f_{LE}, and f_{HE} that simultaneously satisfy eq 2 and the two additional constraints). The bounds on the fractions of total CH_4 emissions from each source in the Barnett Shale determined from this analysis are the following: 41−52% from a high-C_2H_6 fossil source, 0−59% from a low-C_2H_6 fossil source, and 0−48% from a microbial source. These results reveal the importance of a high-C_2H_6 fossil fuel source: Contributing about 45% to total CH_4 emissions in this analysis, a high-C_2H_6 source is required to explain the $flux_{C2H6}$:$flux_{CH4}$ observed on the downwind mass balance flights where the integrated C_2H_6:CH_4 × 100% averages to 5.0%. Because the C_2H_6:CH_4 of the low-C_2H_6 source and the microbial source fall on the same side of the observations (i.e., C_2H_6:CH_4 × 100% < 5.0%), this method cannot partition tightly between those sources. Even with the large range, the upper bound of 48% contribution of microbial sources to total CH_4 emissions is consistent with the most likely estimates (15−29%) determined from the previous analyses. To achieve 48% microbial emissions, zero contribution of a low-C_2H_6 fossil source to total CH_4 emissions is required, which is inconsistent with observations. Combining the CDF and *p*-value analyses with this linear combination approach suggests the CH_4 emissions sources from the studied region of the Barnett Shale are about 20% microbial, about 35% low-C_2H_6 fossil, and about 45% high-C_2H_6 fossil.

Representativity of Source Field for Downwind Observations. Implicit in the use of the C_2H_6:CH_4 measured over the source region (17-Oct. flight) to apportion the integrated, downwind CH_4 enhancements is the assumption that the sampled ratios are representative of emissions from the entire region and are consistent from day-to-day. The validity of this assumption is investigated by simulating transport of emissions from the source region to the location of downwind transects.

In the simulation, the geographic area including the flight path on 17-Oct. is divided into equally spaced sections parallel to the average wind direction (gray lines, Figure 5). The averages of the 17-Oct. observations (either CH_4, C_2H_6, or C_2H_6:CH_4 × 100%) that fall within the longitudinal and latitudinal boundaries of each section are calculated. Dilution

DOI: 10.1021/acs.est.5b00219
Environ. Sci. Technol. 2015, 49, 8158−8166

and turbulent mixing of emissions as they are transported from the source region to the downwind transect are not taken into account in this simple model construct. The latitude/longitude coordinates where the averages determined for each section would be observed if emissions were transported to a given downwind flight path are determined by the point where the center of each section intersects the downwind flight path. Thus, the simulated observations can be plotted along the horizontal flight track and compared to the actual downwind observations (Figure 6 and Figure S8, Suporting Information).

The shapes of simulated compared to observed quantities, shown in Figure 6, generally agree. The success of this simple model to replicate the shape of the downwind observations provides powerful support that the 17-Oct. flight representatively sampled emissions from the Barnett Shale region and that the sampled emissions are representative of the overall CH_4, C_2H_6, and C_2H_6:CH_4 emissions from this region. Furthermore, this analysis indicates that the emissions ratios are consistent and repeatable across multiple days. Although point source emissions in the Barnett Shale region may vary from day-to-day, when observed in aggregate as done here, the net emissions distributions remain consistent. The differences in magnitudes of observed and simulated CH_4 and C_2H_6 are expected because factors influencing dilution of transported emissions are not taken into account in this simple model construct. Assumptions causing imperfect agreement in the simulated shape of all three quantities include the use of a single, average wind speed and a uniform wind direction field.

Implications. We demonstrate that C_2H_6 measurements paired with simultaneous CH_4 measurements over a complex region of high oil and gas production from the Barnett Shale region in Texas allow quantitative attribution of CH_4 emissions. Application of the multiple methods presented herein to the net CH_4 emissions in the Barnett Shale region suggest about 71−85% of CH_4 emissions can be attributed to fossil sources. The concepts and approaches developed and applied here to partitioning of CH_4 emissions in the Barnett Shale can be extended to study other CH_4 emissions regions. However, observational characterization of the C_2H_6:CH_4 source ratios is needed in each location, as different distributions of emissions ratios are expected, even in other oil and gas production regions.

We also present the first tightly constrained C_2H_6 emissions estimates with quantified uncertainty determined using aircraft observations and the mass balance method. Although the average C_2H_6 flux from the Barnett Shale region of $6.6 \pm 0.2 \times 10^3$ kg hr^{-1} is small compared to estimated C_2H_6 emissions within the United States (270×10^3 kg hr^{-1}) and globally (1500×10^3 kg hr^{-1}),[14] emissions may influence local and regional atmospheric composition through production of tropospheric ozone. Well-constrained C_2H_6 fluxes, which in this case exhibit less uncertainty and tighter constraints than methane, likely attributable to the larger signal to background variation, may prove useful for quantifying CH_4 fluxes from regions and sources of known C_2H_6:CH_4.

■ ASSOCIATED CONTENT

Supporting Information

Values used in eq 1. Error in C_2H_6:CH_4 introduced by subsampling C_2H_6. C_2H_6 concentration with altitude. Methods and results for Window and Plume methods. CH_4, C_2H_6, and C_2H_6:CH_4 × 100% for 16-, 25-, and 28-Oct. The Supporting Information is available free of charge on the ACS Publications website at DOI: 10.1021/acs.est.5b00219.

■ AUTHOR INFORMATION

Corresponding Author

*E-mail: eakort@umich.edu. Phone: (734) 763-8414. Fax: (734) 764-0437.

Author Contributions

The manuscript was written through contributions of all authors. All authors have given approval to the final version.

Notes

The authors declare no competing financial interest.

■ ACKNOWLEDGMENTS

This work was supported by in part by the Environmental Defense Fund (EDF) as part of the Barnett Coordinated Campaign, NASA [NNX14AI87G], NOAA [NA14OAR0110139], and the W. M. Keck Institute for Space Studies. We thank J. Marero for measurement and assignment on the Irvine scale[25,28] of C_2H_6 in the compressed air tank (BEth). We thank Stephen Conley (UC Davis), Sonja Wolter (NOAA/CIRES), and Tim Newberger (NOAA/CIRES) for assistance collecting data during the campaign, Ramon Alverez (EDF) for useful comments on the manuscript, and David Lyon (EDF) for providing the well location and production data.

■ REFERENCES

(1) IPCC. *Climate Change 2013: The Physical Science Basis*; Contribution of Working Group I to the Fifth Assessment Report of the Intergovernmental Panel on Climate Change; Cambridge, U.K. and New York, 2013.

(2) U.S. E.P.A.. *Inventory of U.S. Greenhouse Gas Emissions and Sinks: 1990−2011*; Technical Report EPA 430-R-13-001; U.S. Environmental Protection Agency: Washington, DC, 2013.

(3) Miller, S. M.; Wofsy, S. C.; Michalak, A. M.; Kort, E. A.; Andrews, A. E.; Biraud, S. C.; Dlugokencky, E. J.; Eluszkiewicz, J.; Fischer, M. L.; Janssens-Maenhout, G.; et al. Anthropogenic emissions of methane in the United States. *Proc. Natl. Acad. Sci. U.S.A.* **2013**, *110* (50), 20018−20022.

(4) Kort, E. A.; Eluszkiewicz, J.; Stephens, B. B.; Miller, J. B.; Gerbig, C.; Nehrkorn, T.; Daube, B. C.; Kaplan, J. O.; Houweling, S.; Wofsy, S. C. Emissions of CH_4 and N_2O over the United States and Canada based on a receptor-oriented modeling framework and COBRA-NA atmospheric observations. *Geophys. Res. Lett.* **2008**, *35* (18), L18808.

(5) Brandt, A. R.; Heath, G. A.; Kort, E. A.; O'Sullivan, F.; Petron, G.; Jordaan, S. M.; Tans, P.; Wilcox, J.; Gopstein, A. M.; Arent, D.; et al. Methane leaks from North American natural gas systems. *Science* **2014**, *343* (6172), 733−735.

(6) Kirschke, S.; Bousquet, P.; Ciais, P.; Saunois, M.; Canadell, J. G.; Dlugokencky, E. J.; Bergamaschi, P.; Bergmann, D.; Blake, D. R.; Bruhwiler, L.; et al. Three decades of global methane sources and sinks. *Nature Geosci.* **2013**, *6* (10), 813−823.

(7) Kort, E. A.; Frankenberg, C.; Costigan, K. R.; Lindenmaier, R.; Dubey, M. K.; Wunch, D. Four corners: The largest US methane anomaly viewed from space. *Geophys. Res. Lett.* **2014**, *41* (19), 6898−6903.

(8) Kai, F. M.; Tyler, S. C.; Randerson, J. T.; Blake, D. R. Reduced methane growth rate explained by decreased Northern Hemisphere microbial sources. *Nature* **2011**, *476* (7359), 194−197.

(9) Levin, I.; Veidt, C.; Vaughn, B. H.; Brailsford, G.; Bromley, T.; Heinz, R.; Lowe, D.; Miller, J. B.; Poss, C.; White, J. W. C. No inter-hemispheric δ^{13} CH_4 trend observed. *Nature* **2012**, *486* (7404), E3−E4.

DOI: 10.1021/acs.est.5b00219
Environ. Sci. Technol. 2015, 49, 8158−8166

(10) Peischl, J.; Ryerson, T. B.; Brioude, J.; Aikin, K. C.; Andrews, A. E.; Atlas, E.; Blake, D.; Daube, B. C.; de Gouw, J. A.; Dlugokencky, E.; et al. Quantifying sources of methane using light alkanes in the Los Angeles basin, California. *J. Geophys. Res.* **2013**, *118* (10), 4974−4990.
(11) Aydin, M.; Verhulst, K. R.; Saltzman, E. S.; Battle, M. O.; Montzka, S. A.; Blake, D. R.; Tang, Q.; Prather, M. J. Recent decreases in fossil-fuel emissions of ethane and methane derived from firn air. *Nature* **2011**, *476* (7359), 198−201.
(12) Schwietzke, S.; Griffin, W. M.; Matthews, H. S.; Bruhwiler, L. M. P. Natural gas fugitive emissions rates constrained by global atmospheric methane and ethane. *Environ. Sci. Technol.* **2014**, *48* (14), 7714−7722.
(13) Simpson, I. J.; Andersen, M. P. S.; Meinardi, S.; Bruhwiler, L.; Blake, N. J.; Helmig, D.; Rowland, F. S.; Blake, D. R. Long-term decline of global atmospheric ethane concentrations and implications for methane. *Nature* **2012**, *488* (7412), 490−494.
(14) Xiao, Y.; Logan, J. A.; Jacob, D. J.; Hudman, R. C.; Yantosca, R.; Blake, D. R. Global budget of ethane and regional constraints on US sources. *J. Geophys. Res.* **2008**, *113* (D21), D21306.
(15) Rudolph, J. The tropospheric distribution and budget of ethane. *J. Geophys. Res.* **1995**, *100* (D6), 11369−11381.
(16) Blake, D. R.; Rowland, F. S. Global atmospheric concentrations and source strength of ethane. *Nature* **1986**, *321* (6067), 231−233.
(17) Singh, H. B.; Hanst, P. L. Peroxyacetyl nitrate (PAN) in the unpolluted atmosphere: An important reservoir for nitrogen oxides. *Geophys. Res. Lett.* **1981**, *8*, 941−944.
(18) Petron, G.; Frost, G.; Miller, B. R.; Hirsch, A. I.; Montzka, S. A.; Karion, A.; Trainer, M.; Sweeney, C.; Andrews, A. E.; Miller, L.; et al. Hydrocarbon emissions characterization in the Colorado Front Range: A pilot study. *J. Geophys. Res.* **2012**, *117*, D04304.
(19) Karion, A.; Sweeney, C.; Petron, G.; Frost, G.; Hardesty, R. M.; Kofler, J.; Miller, B. R.; Newberger, T.; Wolter, S.; Banta, R.; et al. Methane emissions estimate from airborne measurements over a western United States natural gas field. *Geophys. Res. Lett.* **2013**, *40* (16), 4393−4397.
(20) Caulton, D. R.; Shepson, P. B.; Santoro, R. L.; Sparks, J. P.; Howarth, R. W.; Ingraffea, A. R.; Cambaliza, M. O. L.; Sweeney, C.; Karion, A.; Davis, K. J.; et al. Toward a better understanding and quantification of methane emissions from shale gas development. *Proc. Natl. Acad. Sci. U.S.A.* **2014**, *111* (17), 6237−6242.
(21) Yacovitch, T. I.; Herndon, S. C.; Roscioli, J. R.; Floerchinger, C.; McGovern, R. M.; Agnese, M.; Petron, G.; Kofler, J.; Sweeney, C.; Karion, A.; et al. Demonstration of an ethane spectrometer for methane source identification. *Environ. Sci. Technol.* **2014**, *48* (14), 8028−8034.
(22) Lyon, D.; Zavala-Araiza, D.; Alvarez, R.; Harriss, R.; Palacios, V.; Lan, X.; Talbot, R.; Lavoie, T.; Shepson, P.; Yacovitch, T. Using multi-scale measurements to improve methane emissions estimates from oil and gas operations in the Barnett Shale, Texas: A spatially-resolved emission inventory. 2015, accepted; DOI: 10.1021/es506359c.
(23) Railroad Commission of Texas. http://webapps.rrc.state.tx.us/PDQ/generalReportAction.do (accessed October 21, 2014).
(24) Karion, A.; Sweeney, C.; Kort, E. A.; Shepson, P. B.; Brewer, A.; Cambaliza, M.; Conley, S. C.; Davis, K.; Deng, A.; Hardesty, M. Aircraft-based estimate of total methane emissions from the Barnett Shale region. 2015, accepted; DOI: 10.1021/acs.est.5b00217.
(25) Swanson, A. L.; Blake, N. J.; Atlas, E.; Flocke, F.; Blake, D. R.; Rowland, F. S. Seasonal variations of C_2−C_4 nonmethane hydrocarbons and C_1−C_4 alkyl nitrates at the Summit Research Station in Greenland. *J. Geophys. Res.* **2003**, *108* (D2), 4065.
(26) White, W. H.; Anderson, J. A.; Blumenthal, D. L.; Husar, R. B.; Gillani, N. V.; Husar, J. D.; Wilson, W. E. Formation and transport of secondary air pollutants: Ozone and aerosols in the St. Louis urban plume. *Science* **1976**, *194* (4261), 187−189.
(27) Turner, D. B. *Workbook of Atmospheric Dispersion Estimates*; Ref. AP-26 (NTIS PB 191-482); U.S. Environmental Protection Agency: Research Triangle Park, NC, 1970.
(28) Marrero, J. Personal communication; University of California, Irvine, CA, 2014.

DOI: 10.1021/acs.est.5b00219
Environ. Sci. Technol. 2015, 49, 8158−8166